JACS
JOURNAL OF THE AMERICAN CHEMICAL SOCIETY
Article
pubs.acs.org/JACS

A Biomimetic Copper Water Oxidation Catalyst with Low Overpotential

Teng Zhang,[†,∥] Cheng Wang,[†,‡,∥] Shubin Liu,[§] Jin-Liang Wang,[‡] and Wenbin Lin*[,†]

[†]Department of Chemistry, University of Chicago, 929 E. 57th Street, Chicago, Illinois 60637, United States

[‡]Department of Chemistry, University of North Carolina, Campus Box 3290, Caudill and Kenan Laboratories, Chapel Hill,North Carolina 27599, United States

[§]Research Computing Center, University of North Carolina, Chapel Hill, North Carolina 27599, United States

Supporting Information

ABSTRACT: Simply mixing a Cu(II) salt and 6,6′-dihydroxy-2,2′-bipyridine (H_2**L**) in a basic aqueous solution afforded a highly active water oxidation catalyst (WOC). Cyclic voltammetry of the solution at pH = 12−14 shows irreversible catalytic current with an onset potential of ∼0.8 V versus NHE. Catalytic oxygen evolution takes place in controlled potential electrolysis at a relatively low overpotential of 640 mV. Experimental and computational studies suggest that the **L** ligand participates in electron transfer processes to facilitate the oxidation of the Cu center to lead to an active WOC with low overpotential, akin to the use of the tyrosine radical by Photosystem II to oxidize the $CaMn_4$ center for water oxidation.

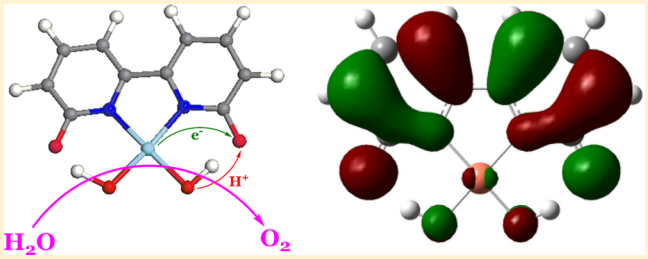

INTRODUCTION

Splitting water into hydrogen and oxygen is one of the most attractive scenarios for solar energy harvesting and sustainable energy production.[1−7] One of the key challenges to water splitting is the development of efficient catalysts for the water oxidation half reaction with low overpotentials, good stability, and high turnover rates.[8,9] Discovering efficient catalysts for the water oxidation reaction has rekindled great interest in recent years, and various molecular and nonmolecular catalysts based on noble[10−17] and earth-abundant[18−28] metals have been reported. Despite much progress in water oxidation catalysis, major improvements in several areas, including lowering overpotentials, increasing catalyst durability, and using earth-abundant elements, are needed before efficient photocatalytic water splitting can be realized.

Recently, copper-based water oxidation catalysts (WOCs) such as the Cu-bipy system,[25] the Cu-carbonate system,[28] and the Cu-peptide system[29] have attracted great interest due to the high abundance and low cost of Cu and the simplicity of these systems. Although these copper-based WOCs show high current densities and good stabilities under basic conditions, difficulties in accessing high-oxidation-state copper species (Cu^{III} and/or Cu^{IV}) lead to high overpotentials for water oxidation and severely limit their practical utility. It is thus highly desirable to identify new strategies to lower overpotentials of these promising Cu-based WOCs.

As in-depth knowledge of the natural water oxidation reaction becomes available,[30−37] more efficient molecular WOCs with lower overpotentials can be designed by mimicking the key features of the water oxidation process in natural photosynthesis. In Photosystem II, a redox-active tyrosine residue, usually referred as tyrosine Z or Y_Z, serves as a mediator in the electron transfer process between the catalytic center, the $CaMn_4$ cluster, and the oxidant, the photochemically generated $P680^+$. Meanwhile, tyrosine Z as well as the adjacent histidine residue His-190 also participates in the "proton-rocking" process, enabling the proton-coupled-electron-transfer (PCET) mechanism for water oxidation reaction.

We report here the use of a ligand containing suitable pendant groups to mimic the functions of tyrosine Z in facilitating the oxidation of the Cu center to lead to a more active WOC. We designed a copper-based WOC with 6,6′-dihydroxy-2,2′-bipyridine (H_2**L**) as the ligand, trying to mimic the role of tyrosine Z in Photosystem II by not only providing a redox-accessible ligand but also having the hydroxyl groups participating in the PCET processes, to lower the overpotential and enhance the WOC activity (Scheme 1). The H_2**L** ligand has been used to synthesize rhodium, ruthenium, and iridium complexes as catalysts for organic transformations,[38−41] CO_2 reduction,[42] and, during the preparation of this Article, water oxidation.[43] The pendant hydroxyl groups were proposed to assist hydride transfer in the catalytic cycles;[42] however, the redox activity of the H_2**L** ligand has not yet been utilized. The idea of using redox active, noninnocent ligands to affect metal reactivities has recently been exploited to enhance catalytic activities,[11,16,44−46] and examples of ligand-assisted proton transfer have also been reported.[47,48]

Received: September 13, 2013
Published: December 10, 2013

dx.doi.org/10.1021/ja409267p | J. Am. Chem. Soc. 2014, 136, 273−281

Scheme 1. Typical PCET Process in Photosystem II (left) and the Proposed Ligand-Assisted PCET in the Cu−L System (right)

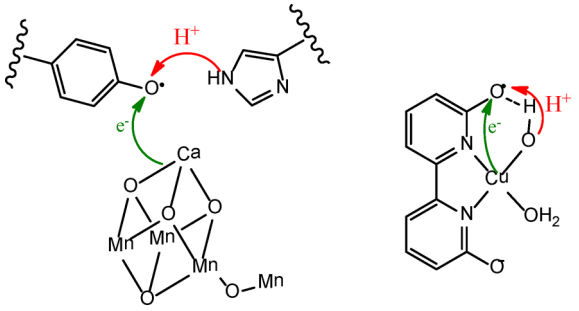

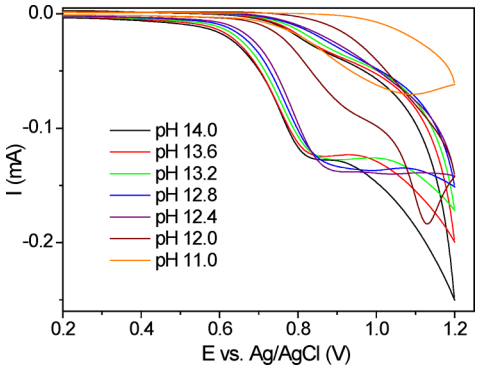

Figure 1. CVs of solutions containing 1 mM of $CuSO_4$ and L^{2-} at various pH's on a glassy carbon electrode (S = 0.07 cm^2).

RESULTS AND DISCUSSION

Electrochemical Water Oxidation of the CuL Complex.

H_2**L** was dissolved in a basic aqueous solution, and a Cu(II) salt (such as $CuSO_4$) was added to form a blue-green solution. Cyclic voltammograms (CVs) were obtained at pH = 11.0−14.0. The CVs showed large, irreversible oxidative waves that correspond to catalytic water oxidation [Figures 1 and S1, Supporting Information (SI)]. In the pH range 11.0−12.2, complicated behaviors were observed, which are attributed to oligmerization or polymerization of the Cu**L** complex. The catalytic currents were well above the background level when the solution contained no catalyst (Figure S2, Supporting Information), showing that the Cu**L** complex is responsible for the catalytic activity. CV of a solution containing only ligand **L** showed the ligand oxidation peak at a similar position (Figure S2, Supporting Information). The water oxidation occurs at a relatively low overpotential (η) of 510−560 mV based on the half-peak potential of the CVs in pH 12.0−14.0, significantly lower than that of the previously reported parent Cu-bipy compound (also denoted as Cu$\mathbf{L}_a$ in Scheme 2) by about 200 mV (Figure 2).[25] This trend is consistent on both glassy carbon and ITO electrodes, though on ITO electrodes the current shows a linear relationship to the potential. The CVs and water oxidation catalytic currents observed for the Cu−**L** system did not depend on the choices of Cu(II) salts or inert electrolyte (Figures S3 and 4, Supporting Information), indicating that the counterions do not coordinate to the Cu centers during the water oxidation reaction.

To verify and quantify the electrochemical oxygen generation, control potential electrolysis (CPE) experiments were carried out at a potential of 0.90 V versus Ag/AgCl reference electrode (1.135 V vs NHE, η = 640 mV) with an ITO electrode in a 0.1 M NaOAc/NaOH solution at pH = 12.4 (Figure 3). A substantial current of >0.15 mA/cm^2 was maintained during the whole period of electrolysis (Figure S5, Supporting Information). The amount of oxygen was determined by gas chromatography, and the Faradaic efficiency was calculated to be (85 ± 5)% based on total charge passing through. CPE experiments under the same pH and the same potential with a catalyst-free solution only gave a current density of 0.003 mA/cm^2 and a negligible amount of oxygen, showing that the copper complex does serve as an effective WOC under such conditions.

CPE experiments were also performed with a large-area glassy carbon electrode. A current density of 0.2 mA/cm^2 was achieved, and a Faradaic efficiency of 59% was calculated on the basis of total charge passing through. The lower Faradaic efficiency is due to oxidation of the carbon electrode (Figure S6, Supporting Information).

Scheme 2. List of 2,2′-Bipyridine Derivatives Used in This Work

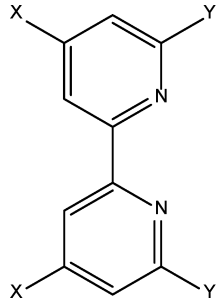

$\mathbf{L}_a$: X = H, Y = H
$H_2\mathbf{L}_b$: X = OH, Y = H
$\mathbf{L}_c$: X = OMe, Y = H
$H_2\mathbf{L}_d$: X = COOH, Y = H

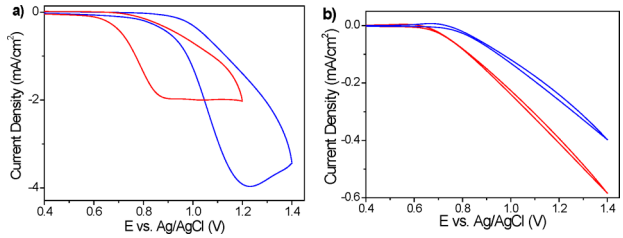

Figure 2. CVs of the Cu-**L** complex (red) and the parent Cu-bipy complex (Cu$\mathbf{L}_a$, blue) in basic aqueous solution (pH = 12.4, 0.1 M NaOH/NaOAc electrolyte) on a glassy carbon electrode (a, S = 0.07 cm^2) and an ITO electrode (b, S = 1 cm^2).

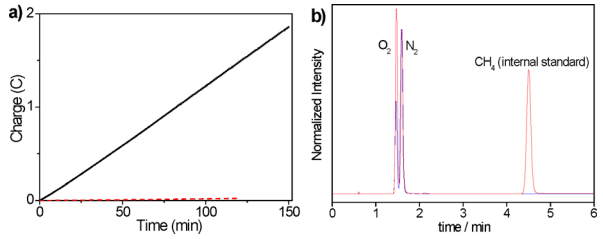

Figure 3. (a) Control potential electrolysis of a solution containing 1 mM catalyst (black solid line) and the buffer only (red dash line) on an ITO electrode (S = 1 cm^2). (b) GC traces from a representative CPE experiment. Blue line shows the air background. Oxygen amount is determined by comparing relative intensity of oxygen and internal standard peaks.

dx.doi.org/10.1021/ja409267p | J. Am. Chem. Soc. 2014, 136, 273−281

The catalyst stability was examined by taking UV−vis spectra before and after electrolysis. When CPE experiments were performed in a fritted cell as in oxygen quantification experiments, little to no depletion of UV−vis signal was observed after 3 h of electrolysis (Figure S7, Supporting Information). An average turnover number of ∼1 O_2/Cu was reached on the basis of the total Cu**L** amount in the solution, but a more realistic TON of ∼400 was estimated on the basis of the amount of Cu**L** involved in electrolysis (Supporting Information).[49] We also recovered the free ligand H_2**L** by first acidifying the solution and then precipitating H_2**L** by removing Cu(II) ions with silica-supported triamine tetraacetate. NMR spectroscopy (Figure S8, Supporting Information) indicated the recovery of >90% of the H_2**L** ligand, which not only supports the catalytic nature of the electrolysis and stability of the complex but also proves water (hydroxide) as the source of oxygen. However, when electrolysis was performed in a spectroelectrochemical cell with no frit or membrane to separate the electrode compartments, the ligand absorption maxima in the UV−vis spectra decreased by ∼30% after the same operating time and a similar turnover number based on bulk concentration (Figure S9, Supporting Information). The catalyst loss is thus attributed to reduction of Cu(II) ions on the counter electrode, releasing free ligand which is readily oxidized. Similar Cu(II) reduction was also observed for the Cu-$\mathbf{L}_a$ system on the counter electrode.[25]

During electrolysis, a deposit was observed on the electrode. Further studies prove that the film is oligomer or polymer of the Cu**L** complex instead of metal oxide. First, the freshly deposited film showed catalytic water oxidation activity in a fresh pH 12.4 buffer without the catalyst, but dissolved back into the solution after 30 min of electrolysis. By taking UV−vis spectra (Figure S10, Supporting Information) and ICP-MS analyses of the solution of the dissolved film, a Cu/**L** ratio of 1.12 ± 0.15 was determined, indicating that the film is likely a coordination polymer containing the ligand as well as Cu, but not copper oxides or hydroxides. Second, the film formation was not observed at higher pH's. If copper oxide or hydroxide is present, its formation should be facilitated by a higher base concentration, which is opposite to our observation.

The electrochemical deposit behaves differently from a direct deposit of the Cu**L** complex on an ITO electrode prepared by drying a methanol solution of Cu-**L** via solvent evaporation. The direct deposit readily dissolves in a basic solution, while the electrochemical deposit only dissolves when a potential bias high enough to drive water oxidation is applied as described above. This different behavior can be explained by partial oxidation of the electrochemical deposit which would make the coordination polymer less soluble. Additional catalytic cycles are needed to return the coordination polymer to its "original" state (i.e., the reduced state) before it can dissolve in a basic solution.

At longer electrolysis time the film grows thicker to form an insulating layer on the electrode, leading to a decrease of electrolysis current. Such "thick" films have Cu/**L** ratios larger than 1, indicating ligand decomposition in the deposit. This at least partially explains the lower Faradaic efficiency for the Cu-**L** system when compared to other copper-based water oxidation systems.

CVs were recorded at different scan rates in order to obtain kinetic information of the Cu-**L** system (Figure 4a). It is convenient to compare the catalytic current to a reversible diffusive current, which is given by eq 1:[50]

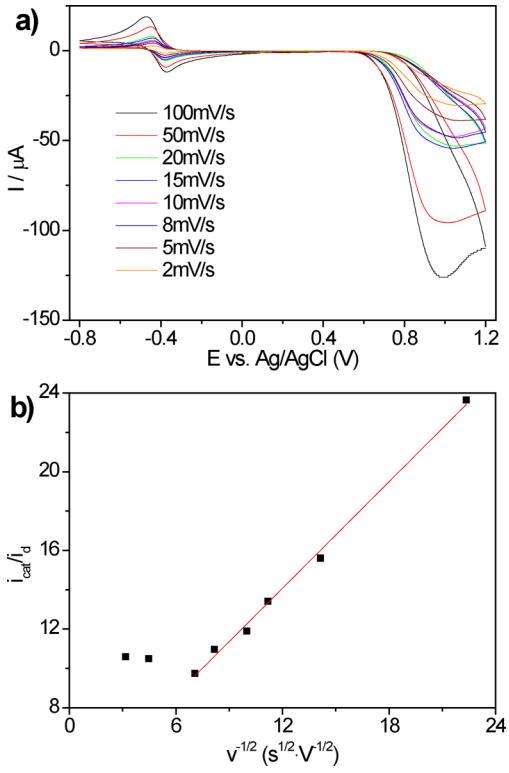

Figure 4. (a) CVs of a 1 mM Cu**L** solution under various scan rates on a glassy carbon electrode (S = 0.07 cm^2, pH 12.4, 0.1 M NaOH/NaOAc, background corrected). (b) Linear fitting plot of i_{cat}/i_d vs $v^{-1/2}$ for TOF calculations.

$$i_d = 0.4633nFAc\sqrt{\frac{nFvD}{RT}} \quad (1)$$

Here, n is the electron transferred in the noncatalytic reaction, F is Faraday's constant, A is the area of the electrode, c is the bulk concentration, v is the scan rate, D is the diffusion coefficient, R is the gas constant, and T is the absolute temperature.

The diffusive peak current in the absence of catalytic processes was estimated using the diffusion-controlled Cu(II)/Cu(I) peak at ∼−0.4 V versus Ag/AgCl (Figure 4a). The Cu(II)/Cu(I) peak is quasireversible at high scan rates (100 mV/s and 50 mV/s) while reversible at low scan rates (≤20 mV/s). The ratio of the catalytic current over the diffusive peak current, i_{cat}/i_d, matches the trend from a pure diffusion behavior (DP) region to a pure kinetic behavior (KP) region as scan rates decrease (Figure 4b).[50] In the KP region, the catalytic peak current in cyclic voltammetry is given by eq 2:[50]

$$i_{cat} = n_{cat}FAc_{cat}\sqrt{k_{cat}D} \quad (2)$$

Here, n_{cat} = 4 is the number of electrons transferred in the catalytic reaction (water oxidation), c_{cat} is the bulk catalyst concentration, k_{cat} is the apparent first-order rate constant, and D is the diffusion coefficient of the catalyst.

By taking the ratio of eq 2 over eq 1 and plugging in all of the constants, we obtain eq 3:

$$\frac{i_{cat}}{i_d} = 1.424\sqrt{\frac{k_{cat}}{v}} \quad (3)$$

The pseudo-first-order rate constant of the catalytic water oxidation (or hydroxide oxidation at high pH), k_{cat}, is usually

dx.doi.org/10.1021/ja409267p | J. Am. Chem. Soc. 2014, 136, 273−281

referred as turnover frequency (TOF) of the catalyst in the literature. From the slope of the plot of i_{cat}/i_d versus $\nu^{-1/2}$, an apparent k_{cat} = 0.4 s^{-1} was calculated. This value is comparable to most reported molecular water oxidation catalysts,[14,22,51] yet much lower than the recently reported copper based ones.[25,29] However, as the 4-electron water oxidation reaction is much more complicated than the simplified model of E_rC_{cat} reaction, the calculated k_{cat} value can only serve as an estimate of the catalytic rate.

Characterization of Aqueous Species in Cu-L Solutions. Small needle-like crystals were observed by adjusting the pH of an aqueous Cu**L** solution from highly basic conditions (pH > 12) to ~11.0. These crystals are of the same phase as single crystals of a coordination polymer grown from a mixed methanol/water solution as indicated by their identical PXRD patterns (Figure S14, Supporting Information). A single crystal X-ray diffraction study shows that, in the crystal, the Cu center and the **L** ligand form 1-D coordination polymer with the formula $[Cu(H\mathbf{L})(\mu_2\text{-}OH)]_n$. In the crystal structure, each Cu center adopts a slightly distorted square planar coordination environment with a monodeprotonated ligand $H\mathbf{L}^-$ and two bridging hydroxo groups. Two oxygen atoms from two adjacent H**L** ligands sit at the axial positions with Cu−O distances of 2.690(3) and 3.076(4) Å, respectively, showing very weak interactions with the Cu center. The O···O distances between a μ-hydroxo group and its nearest neighbors from the $H\mathbf{L}^-$ ligands are 2.452(5) and 2.497(4) Å, respectively, indicating the existence of hydrogen bonding (Figure 5 and Figure S15, Supporting Information).

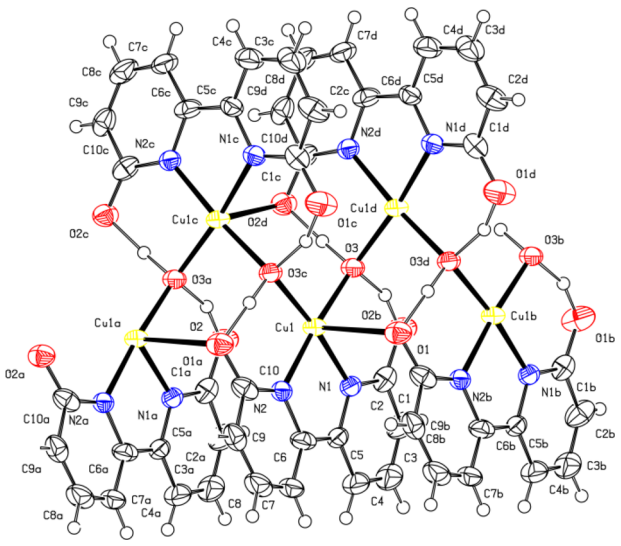

Figure 5. X-ray structure of 1-D polymer $[Cu(H\mathbf{L})(OH)]_n$. Atoms shown at 50% probability: red, O; blue, N; yellow, Cu; white, C.

We observed precipitate formation at pH 12.4 when the concentration of the Cu**L** complex exceeded 2 mM, suggesting the presence of an equilibrium between monomer and oligomer/polymer species in solution. Hydroxo-bridged dinuclear species are well-known for Cu-bipy or Cu-diamine complexes in neutral to weakly basic aqueous solutions.[52−55] However, in the Cu-**L** system, formation of the $Cu_2(\mu_2\text{-}OH)_2$ dimer is less favorable due to the steric effect of the 6,6′-substituents. Formation of oligomer or polymer is thus favored because less steric hindrance is experienced in the oligomer/polymer species. The presence of polynuclear species was also supported by ESI-MS studies (Figure S16, Supporting Information). An equilibrium between monomer and oligomer/polymer species also accounts for an unusual trend of concentration-dependent CVs, in which the catalytic peak currents showed a curving-over behavior at high Cu**L** concentrations (Figure 6). This equilibrium is also proposed to be responsible for the film formation, presumably owing to the local pH decrease during the control potential electrolysis.

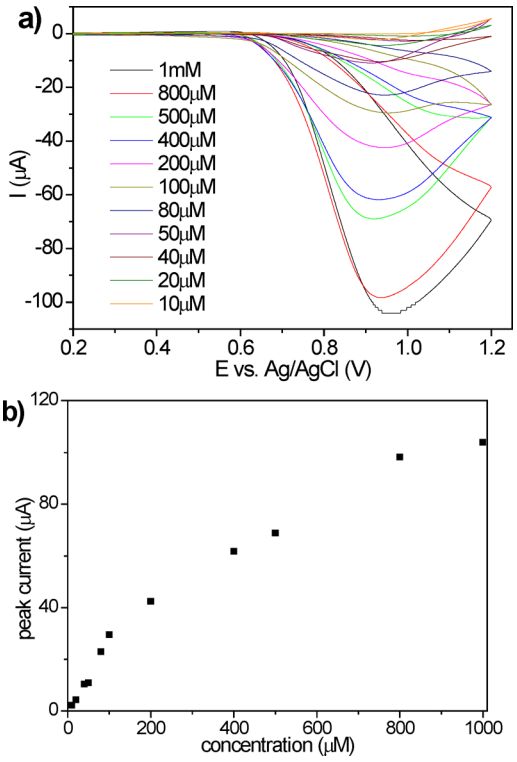

Figure 6. (a) CVs of Cu**L** solutions at various concentrations on a glassy carbon electrode (S = 0.07 cm^2, pH 12.4, 0.1 M NaOH/NaOAc, ν = 100 mV/s, background corrected). (b) The relationship between the concentration and CV peak current of the Cu**L** complex.

A titration curve of the Cu-**L** system was also obtained (Figure 7). At the initial state, the $H_2\mathbf{L}$ ligand did not dissolve in water. It slowly dissolved upon addition of base and began to form a blue-green complex with the Cu(II) ion. However, a blue-green precipitate formed after ~1.5 equiv of base was

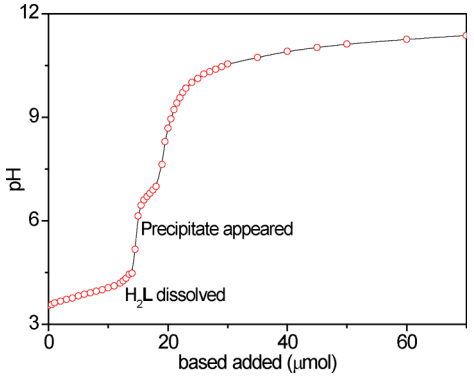

Figure 7. Titration curve of 10 mL of 1 mM Cu/$H_2\mathbf{L}$ solution.

dx.doi.org/10.1021/ja409267p | J. Am. Chem. Soc. 2014, 136, 273−281

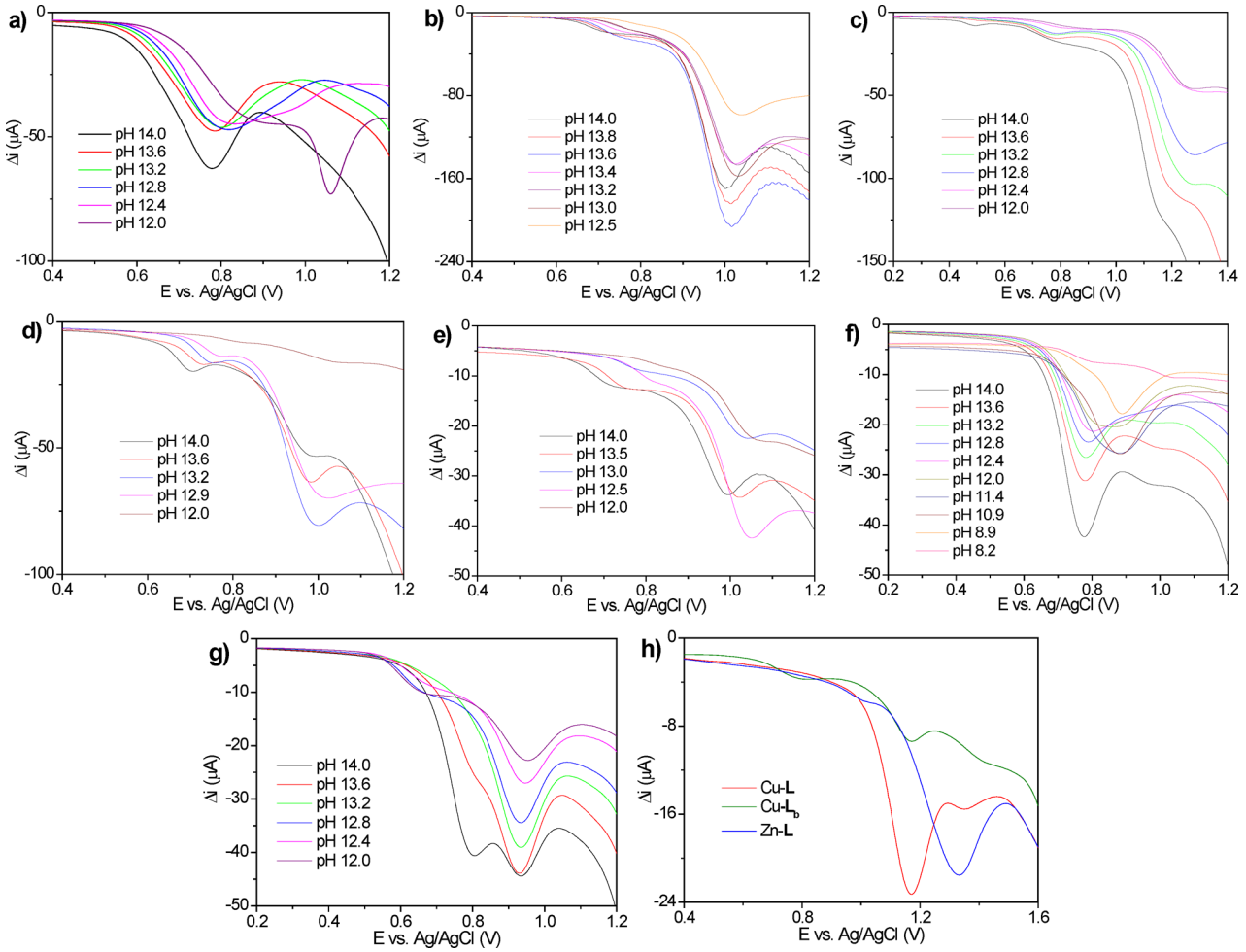

Figure 8. SWVs of aqueous solutions containing 1 mM of (a) Cu^{2+} and L^{2-}; (b) Cu^{2+} and L_a; (c) Cu^{2+} and L_b^{2-}; (d) Cu^{2+} and L_c; (e) Cu^{2+} and L_d^{2-}; (f) L^{2-}; (g) Zn^{2+} and L^{2-} under various pH's (glassy carbon electrode, S = 0.07 cm^2, 1 M KOH/KNO_3). (h) SWVs of 1 mM CuL, CuL_b, and ZnL in mix DMF/H_2O solution with 2 equiv of KOH (glassy carbon electrode, S = 0.07 cm^2, 0.1 M NMe_4BF_4).

added, and a titration jump was observed. This is attributed to dimerization or polymerization of the $Cu(HL)^+$ and CuL complexes. A second titration jump was observed upon addition of ~2 equiv of base, indicating a complete transformation to the neutral $[Cu(HL)(OH)]_n(OH_2)_x$ polymer. The precipitate, presumably the neutral polymer, did not fully dissolve until excess (>20 equiv) of base was added. The titration experiment thus indicates that an anionic species, $CuL(OH)(OH_2)^-$, is the dominant species in the catalytically active solution, and possibly the true catalyst.

Electrochemistry of Analogous Systems. In order to elucidate the water oxidation mechanism and the reason for the lower overpotential observed for the Cu-L system, we carried out electrochemical studies on the M-L systems as well as related M-bipy systems. Scheme 2 shows a list of the 2,2′-bipy derivatives we examined. Square wave voltammetry (SWV) was used instead of CV because it better identifies the positions of redox peaks due to its higher sensitivity, and it also gives redox potentials under catalytic conditions.[56,57]

SWVs of CuL complex under the same conditions as CVs showed a pH-dependent peak between 1.01 and 1.07 V versus NHE (Figure 8a). As indicated by CVs and CPE experiments, this peak is responsible for catalytic water oxidation. Peaks at higher potentials were observed at lower pH's, which are attributed to protonation and polymerization of the copper species.

Interestingly, CuL serves as the only example with water oxidation observed at a lower overpotential than the parent CuL_a complex. SWVs of the parent complex $CuL_a(OH)_2$ in basic aqueous solution show a small, pH-dependent peak between 0.93 and 1.03 V versus NHE (Figure 8b) which is attributed to the Cu(III)/Cu(II) redox pair. A second oxidation occurs at around ~1.23 V versus NHE and leads to catalytic water oxidation. Similar behaviors were observed in 4,4′-substituted systems Cu-L_c and Cu-L_d (Figure 8d,e). Both the Cu(III)/Cu(II) peak and the water oxidation peak are only slightly affected by substituents at 4,4′ positions, consistent with the previous report by Mayer and co-workers.[25]

Surprisingly, Cu(II) complex of the 4,4′-substituted analogue of H_2L, 4,4′-dihydroxy-2,2′-bipyridine (H_2L_b), showed an even higher overpotential for water oxidation than the parent complex $CuL_a(OH)_2$ as indicated by SWVs (Figure 8b,c). The differences between CuL and CuL_b complexes indicate that the lower overpotential observed in the CuL complex is not simply due to the electron-donating nature of the substituents or introduction of additional negative charge.

To further investigate the roles of 6,6′-substituted hydroxyl groups in water oxidation, SWVs were also recorded in a DMF/H_2O (v/v 9:1) solution to reduce the catalytic signal. A 1 equiv

dx.doi.org/10.1021/ja409267p | J. Am. Chem. Soc. 2014, 136, 273−281

portion of copper trifluorosulfonate or zinc trifluorosulfonate, 1 equiv of H_2**L** or H_2**L**$_b$ ligand, and 2 equiv of KOH were dissolved in the DMF/H_2O mixed solvent to afford a solution with a metal concentration of 1 mM. Two sequential redox peaks were observed in the Cu-**L** solution at 1.18 and 1.35 V versus Ag/AgCl, while only the first peak was observed in the Cu-**L**$_b$ solution (Figure 8h). Thus, the first peak was assigned to the Cu(III)/Cu(II) redox pair. An additional redox peak was also observed in the Cu-**L**$_b$ solution at 0.82 V versus Ag/AgCl, which could be assigned to some DMF-coordinated copper species. The second peak was assigned to ligand oxidation by comparing to the Zn-**L** system, for which a redox peak was observed at 1.33 V versus Ag/AgCl (Figure 8h). As the ligand oxidation potential is very close to the Cu(III)/Cu(II) potential, we propose that ligand oxidation is involved in the catalytic cycle and plays a key role in lowering the overpotential for water oxidation.

We also compared SWVs of the Cu**L** complex with free ligand $\mathbf{L}^{2-}$/$\mathbf{HL}^{-}$ and analogous Zn**L** complex in aqueous solution to confirm the ligand oxidation in catalytic cycle. Free ligand shows pH-independent oxidation peak at ~1.01 V vs NHE between pH 14.0 and 12.8, and shifts to ~1.12 V versus NHE between pH 12.8 and 9.0. The shift on peak position is attributed to the protonation from $\mathbf{L}^{2-}$ to $\mathbf{HL}^{-}$. A second protonation was observed around pH 8.5 as indicated by another peak position shift, corresponding to the protonation from $\mathbf{HL}^{-}$ to H_2**L** (Figure 8f). The second protonation is consistent with the titration curve of $\mathbf{L}^{2-}$ (Figure S18, Supporting Information), and both protonation steps are consistent with a change on UV–vis spectra (Figure 9). The

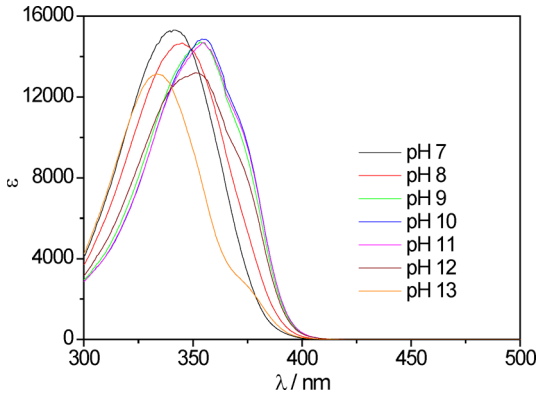

Figure 9. UV–vis spectra of free $\mathbf{L}^{2-}$ ligand in aqueous solution at various pH's.

Zn**L** complex shows a pH-independent redox peak at ~1.16 V versus NHE (Figure 8g). We propose that the dominant species of the Zn**L** complex is Zn**L**$(OH)(OH_2)^{-}$ as indicated by a titration curve (Figure S20, Supporting Information), and assign the redox peak to the ligand oxidation of the species.

As shown in Figure 8f,g, the oxidation of the **L** ligand is little affected by metal coordination when the metal complexes bear the same charge as the protonated free ligand. It could be explained by the structural similarity between $\mathbf{HL}^{-}$ and Cu**L** or Zn**L** complexes. The pH-dependent UV–vis spectra of the free ligand (Figure 9) show a blue shift of the absorption maximum upon protonation from $\mathbf{L}^{2-}$ to $\mathbf{HL}^{-}$, and a red shift upon protonation from $\mathbf{HL}^{-}$ to H_2**L**. The UV–vis spectra of Cu**L** and Zn**L** complexes show absorption peaks at a similar position as $\mathbf{HL}^{-}$ (Figure S21, Supporting Information). The similarity of the UV–vis spectra of $\mathbf{HL}^{-}$ and Cu**L** or Zn**L** complexes suggests similarity of their structures. A planar structure of the monoprotonated form $\mathbf{HL}^{-}$ is proposed (Scheme 3), which is

Scheme 3. Proposed Structures for Mono-Deprotonated and Di-Deprotonated forms of H_2L

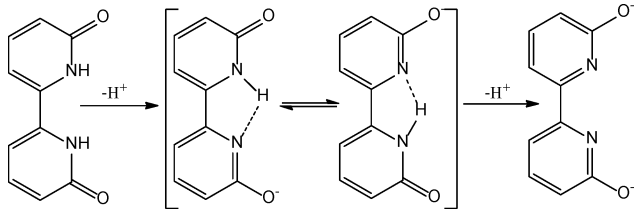

corroborated by DFT calculations (Figure S22, Supporting Information). Given similar structures of $\mathbf{HL}^{-}$ and Cu**L** or Zn**L** complexes and similar electronic effects of H^+, Cu(OH)$(OH_2)^+$, and Zn(OH)$(OH_2)^+$, it is not surprising to see similar ligand oxidation potentials of the three.

Computational Studies on the Catalysis Mechanism. The catalytic cycle for water oxidation is proposed in Scheme 4b. DFT calculations were performed on the Cu-**L** complex for a better understanding of the water oxidation mechanism. As shown in Scheme 4a, the redox active $\mathbf{L}^{2-}$ ligand plays an important role in the second oxidation step from a Cu(III) species to an apparent "Cu(IV)" species. As shown by calculation results, in the parent Cu-bipy complex the second oxidation can only take place at the hydroxo group with a calculated oxidation potential of 1.4 V versus NHE due to the difficulty in oxidizing the bipy ligand (Scheme S1, Supporting Information). However, in the Cu-**L** complex, the second oxidation takes place at the ligand as indicated by the ligand-centered singly occupied molecular orbital (SOMO) of **9** (Figure 10). The calculated spin density (Figure 10) of **9** mainly locates at the ligand, indicating that it is more like a Cu(III) species with the ligand having the radical character. By involving the ligand in the oxidation process, the second redox potential is lowered by ~0.3 V as indicated by the DFT calculations compared to the corresponding oxidation step for the parent Cu-bipy complex (Scheme 4 and Scheme S1, Supporting Information), leading to stabilization of the highly oxidized intermediate. Thus, the redox active $\mathbf{L}^{2-}$ ligand serves as an electron transfer mediator in the catalytic cycle and is responsible for the low overpotential observed, and water oxidation is found to be driven by a Cu(III) center other than a harder-to-access Cu(IV) one. However, as the oxyl-centered radical character of a Cu(IV)-oxo species[58] (i.e., **6′** in the Cu-bipy system, Scheme S1, Supporting Information) makes it more electrophilic and reactive than the Cu(III)-hydroxyl species **9**, the formation of peroxo species **11** (Scheme 4b), which is believed to be the rate determining step of the water oxidation process, is probably disfavored in the case of the Cu-**L** complex. This could in part explain the lower current density and the slower TOF value for the Cu-**L** complex compared to the parent Cu-bipy system (Figure 2a).

Calculation on the Cu-**L**$_b$ system uncovers why the Cu**L**$_b$ complex does not serve as an effective water oxidation catalyst as Cu**L**. Although Cu**L**$_b$$(OH)(OH_2)^{-}$ exhibits a lower Cu(III)/Cu(II) redox potential, the second oxidation on ligand is ~0.2 V higher than the 6,6′-substituted analogue (Scheme S2, Supporting Information), consistent with the electrochemical behaviors observed in both aqueous and nonaqueous solutions.

dx.doi.org/10.1021/ja409267p | J. Am. Chem. Soc. 2014, 136, 273–281

Scheme 4. (a) Calculated Thermodynamic Pathways for the First and Second Oxidation of the Cu-L Complex[a] and (b) Proposed Mechanism for Water Oxidation

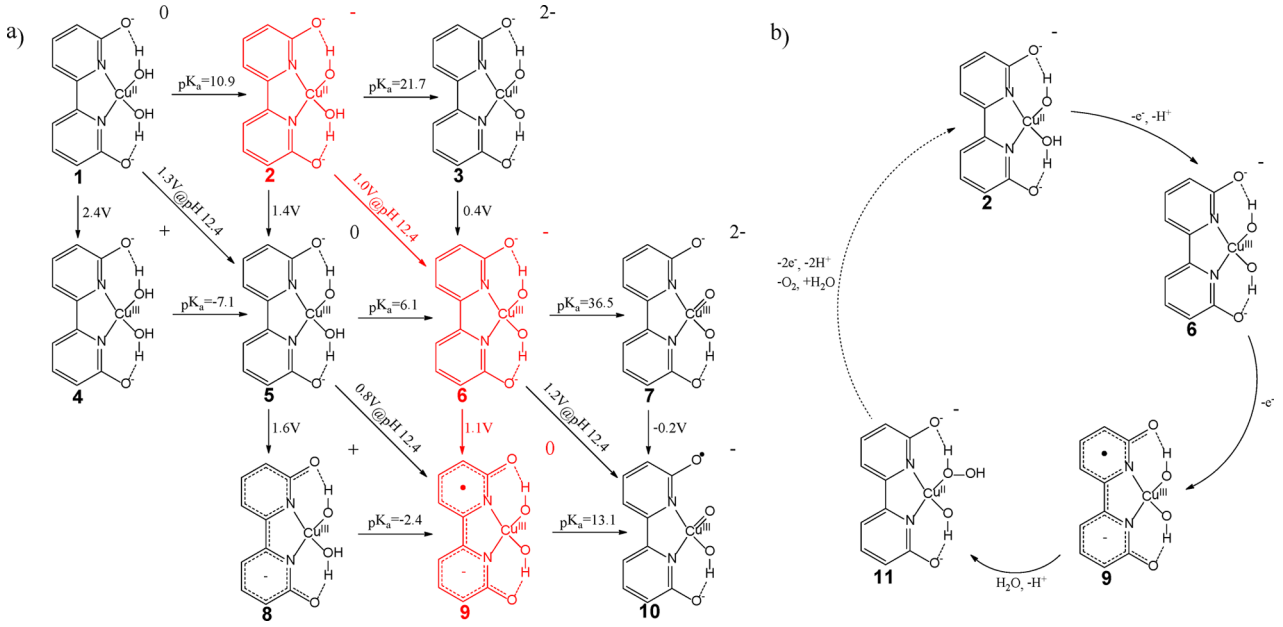

[a]Structures in red indicate the proposed most probable pathway based on DFT calculations. Redox potential values are reported vs NHE.

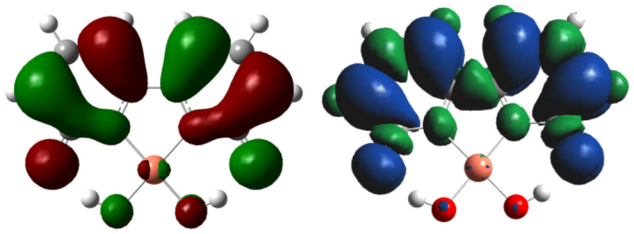

Figure 10. Calculated SOMO (left) and spin density (right) of structure **9**.

The higher ligand oxidation potential for $\mathbf{L_b}$ thus explains why $\mathbf{CuL_b}$ exhibits a higher overpotential for water oxidation.

However, we should note that accurate prediction of pK_a's and redox potentials is still a challenging problem with calculated values significantly deviating from experimental ones. Thus, the absolute values of the calculated pK_a's and redox potentials are not so informative. Fortunately, the trends we obtained from calculations on the Cu-**L**, Cu-bipy, and Cu-$\mathbf{L_b}$ systems match with our experimental results, lending support to our conclusions.

CONCLUDING REMARKS

The introduction of 6,6′-dihydroxyl groups on the bipy moiety allows the **L** ligand to be intimately involved in the water oxidation catalytic cycle via ligand oxidation and significantly lowers the water oxidation overpotential. This work thus uncovers an effective biomimetic strategy toward ligand design for preparing highly efficient WOCs.

Due to the difficulty in characterizing the intermediates in electrocatalysis, we were not able to experimentally prove or disprove the intramolecular PCET process. Further experimental and theoretical studies are under way to fully unravel the detailed mechanisms and to design more efficient WOCs based on our knowledge of this biomimetic strategy.

EXPERIMENTAL SECTION

Electrochemistry and Gas Analysis. Cyclic voltammograms (CVs), square wave voltammograms (SWVs), and controlled potential electrolysis (CPE) were recorded on a CHI420 electrochemistry workstation. Regular 3-electrode systems were used. CVs and SWVs were recorded using a glassy carbon disk working electrode (S = 0.07 cm^2) unless noted. Bulk electrolysis was performed in a gastight fritted cell to separate the cathode and the anode. No further calibration on iR drop was applied. A Ag/AgCl/1 M KCl electrode was used as the reference electrode in all experiments, and its potential (0.235 V vs NHE) was calibrated with the $Fe(CN)_6^{3-}$/ $Fe(CN)_6^{4-}$ couple.[59] For CVs and SWVs in aqueous solution, the electrolyte (1 M) was prepared by titrating 1 M KOH solution with HNO_3 to the desired pH. A 0.1 M solution of NMe_4BF_4 in DMF/H_2O (90:10, v/v) was used for nonaqueous CVs and SWVs. The pH 12.4 buffer was prepared by dissolving NaOH (0.025 M) and the inert salt (NaOAc, $NaNO_3$, or $NaClO_4$, 0.075 M) in the same solution and then adjusting to the desired pH with the corresponding acid. Analysis of the gas product in CPE experiments was conducted by gas chromatography (Varian 450-GC, molecular sieve columns, pulsed discharge helium ionization detector, PDHID). Background from air was calibrated with respect to the nitrogen signal, and the amount of oxygen was determined by comparing to a methane internal standard.

Computational Details. All quantum chemical calculations were performed using the density functional theory (DFT) functional B3LYP/6-311G+g(d) as implemented in the Gaussian 09 software suite.[60] Open-shell and closed-shell electronic structure complexes were optimized at the unrestricted and restricted level, respectively. Solvation was considered in the calculations using the conductor-like polarizable continuum model (CPCM).

pK_a's and redox potentials were calculated from free energy values obtained from frequency calculations. Reference potential of NHE was set at 4.28 V for redox potential calculation, while standard free energy of proton was set at −11.72 eV for pK_a calculation as reported in the literature.[61]

ASSOCIATED CONTENT

Supporting Information

Crystallographic data (CIF), detailed experimental procedure, synthesis of compound $H_2\mathbf{L}$, calculation of TON in electrolysis,

dx.doi.org/10.1021/ja409267p | J. Am. Chem. Soc. 2014, 136, 273−281

additional CVs and electrolysis data of Cu-**L** solutions, ESI-MS spectrum of Cu-**L**, ICP-MS results and UV−vis spectra of the film, table of redox potentials for SWVs in Figure 8, titration curves of $\mathbf{L}^{2-}$, Cu-$\mathbf{L}_b$ and Zn-**L** solutions, UV−vis spectra of Cu-**L** and Zn-**L** solutions, and computational results of Cu-$\mathbf{L}_a$ and Cu-$\mathbf{L}_b$ systems. Complete ref 60. This material is available free of charge via the Internet at http://pubs.acs.org.

AUTHOR INFORMATION

Corresponding Author

wenbinlin@uchicago.edu.

Author Contributions

‖These authors contributed equally.

Notes

The authors declare no competing financial interest.

ACKNOWLEDGMENTS

We thank the NSF-DMR for funding support. C.W. gratefully acknowledges the UNC Department of Chemistry for an Ernest L. Eliel fellowship and a Venable award. We thank Mr. Christopher Poon and Ms. Stephanie A. Kramer for ICP-MS experiments. We thank Dr. Sohrab Habibi for ESI-MS experiments.

REFERENCES

(1) Fujishima, A.; Honda, K. *Nature* **1972**, *238*, 37.
(2) Youngblood, W. J.; Lee, S. A.; Kobayashi, Y.; Hernandez-Pagan, E.; Hoertz, P. G.; Moore, T. A.; Moore, A. L.; Gust, D.; Mallouk, T. E. *J. Am. Chem. Soc.* **2009**, *131*, 926.
(3) Ohno, T.; Bai, L.; Hisatomi, T.; Maeda, K.; Domen, K. *J. Am. Chem. Soc.* **2012**, *134*, 8254.
(4) Reece, S. Y.; Hamel, J. A.; Sung, K.; Jarvi, T. D.; Esswein, A. J.; Pijpers, J. J. H.; Nocera, D. G. *Science* **2011**, *334*, 645.
(5) Wang, X.; Xu, Q.; Li, M.; Shen, S.; Wang, X.; Wang, Y.; Feng, Z.; Shi, J.; Han, H.; Li, C. *Angew. Chem., Int. Ed.* **2012**, *51*, 13089.
(6) Gao, Y.; Ding, X.; Liu, J.; Wang, L.; Lu, Z.; Li, L.; Sun, L. *J. Am. Chem. Soc.* **2013**, *135*, 4219.
(7) Swierk, J. R.; Mallouk, T. E. *Chem. Soc. Rev.* **2013**, *42*, 2357.
(8) Eisenberg, R.; Gray, H. B. *Inorg. Chem.* **2008**, *47*, 1697.
(9) Barber, J. *Chem. Soc. Rev.* **2009**, *38*, 185.
(10) Hara, M.; Waraksa, C. C.; Lean, J. T.; Lewis, B. A.; Mallouk, T. E. *J. Phys. Chem. A* **2000**, *104*, 5275.
(11) Wada, T.; Tsuge, K.; Tanaka, K. *Inorg. Chem.* **2001**, *40*, 329.
(12) McDaniel, N. D.; Coughlin, F. J.; Tinker, L. L.; Bernhard, S. *J. Am. Chem. Soc.* **2008**, *130*, 210.
(13) Concepcion, J. J.; Jurss, J. W.; Brennaman, M. K.; Hoertz, P. G.; Patrocinio, A. O. T.; Murakami Iha, N. Y.; Templeton, J. L.; Meyer, T. J. *Acc. Chem. Res.* **2009**, *42*, 1954.
(14) Hull, J. F.; Balcells, D.; Blakemore, J. D.; Incarvito, C. D.; Eisenstein, O.; Brudvig, G. W.; Crabtree, R. H. *J. Am. Chem. Soc.* **2009**, *131*, 8730.
(15) Duan, L.; Bozoglian, F.; Mandal, S.; Stewart, B.; Privalov, T.; Llobet, A.; Sun, L. *Nat. Chem.* **2012**, *4*, 418.
(16) Kärkäs, M. D.; Åkermark, T.; Johnston, E. V.; Karim, S. R.; Laine, T. M.; Lee, B.; Åkermark, T.; Privalov, T.; Åkermark, B. *Angew. Chem., Int. Ed.* **2012**, *51*, 11589.
(17) Wang, C.; Wang, J.; Lin, W. *J. Am. Chem. Soc.* **2012**, *134*, 19895.
(18) Kanan, M. W.; Nocera, D. G. *Science* **2008**, *321*, 1072.
(19) Dismukes, G. C.; Brimblecombe, R.; Felton, G. A. N.; Pryadun, R. S.; Sheats, J. E.; Spiccia, L.; Swiegers, G. F. *Acc. Chem. Res.* **2009**, *42*, 1935.
(20) Jiao, F.; Frei, H. *Angew. Chem., Int. Ed.* **2009**, *48*, 1841.
(21) Yin, Q.; Tan, J. M.; Besson, C.; Geletii, Y. V.; Musaev, D. G.; Kuznetsov, A. E.; Luo, Z.; Hardcastle, K. I.; Hill, C. L. *Science* **2010**, *328*, 342.
(22) Ellis, W. C.; McDaniel, N. D.; Bernhard, S.; Collins, T. J. *J. Am. Chem. Soc.* **2010**, *132*, 10990.
(23) Wasylenko, D. J.; Ganesamoorthy, C.; Borau-Garcia, J.; Berlinguette, C. P. *Chem. Commun.* **2011**, *47*, 4249.
(24) Fillol, J. L.; Codolà, Z.; Garcia-Bosch, I.; Gómez, L.; Pla, J. J.; Costas, M. *Nat. Chem.* **2011**, *3*, 807.
(25) Barnett, S. M.; Goldberg, K. I.; Mayer, J. M. *Nat. Chem.* **2012**, *4*, 498.
(26) Zhang, F.; Yamakata, A.; Maeda, K.; Moriya, Y.; Takata, T.; Kubota, J.; Teshima, K.; Oishi, S.; Domen, K. *J. Am. Chem. Soc.* **2012**, *134*, 8348.
(27) Trotochaud, L.; Ranney, J. K.; Williams, K. N.; Boettcher, S. W. *J. Am. Chem. Soc.* **2012**, *134*, 17253.
(28) Chen, Z.; Meyer, T. J. *Angew. Chem., Int. Ed.* **2013**, *52*, 700.
(29) Zhang, M.; Chen, Z.; Kang, P.; Meyer, T. J. *J. Am. Chem. Soc.* **2013**, *135*, 2048.
(30) Kok, B.; Forbush, B.; McGloin, M. *Photochem. Photobiol.* **1970**, *11*, 457.
(31) Zouni, A.; Witt, H.; Kern, J.; Fromme, P.; Krauss, N.; Saenger, W.; Orth, P. *Nature* **2001**, *409*, 739.
(32) Ferreira, K. N.; Iverson, T. M.; Maghlaoui, K.; Barber, J.; Iwata, S. *Science* **2004**, *303*, 1831.
(33) Loll, B.; Kern, J.; Saenger, W.; Zouni, A.; Biesiadka, J. *Nature* **2005**, *438*, 1040.
(34) McEvoy, J. P.; Brudvig, G. W. *Chem. Rev.* **2006**, *106*, 4455.
(35) Umena, Y.; Kawakami, K.; Shen, J.; Kamiya, N. *Nature* **2011**, *473*, 55.
(36) Klauss, A.; Haumann, M.; Dau, H. *Proc. Natl. Acad. Sci.* **2012**, *109*, 16035.
(37) Cox, N.; Pantazis, D. A.; Neese, F.; Lubitz, W. *Acc. Chem. Res.* **2013**, *46*, 1588.
(38) Conifer, C. M.; Taylor, R. A.; Law, D. J.; Sunley, G. J.; White, A. J. P.; Britovsek, G. J. P. *Dalton Trans.* **2011**, *40*, 1031.
(39) Conifer, C. M.; Law, D. J.; Sunley, G. J.; Haynes, A.; Wells, J. R.; White, A. J. P.; Britovsek, G. J. P. *Eur. J. Inorg. Chem.* **2011**, *2011*, 3511.
(40) Nieto, I.; Livings, M. S.; Sacci, J. B.; Reuther, L. E.; Zeller, M.; Papish, E. T. *Organometallics* **2011**, *30*, 6339.
(41) Kawahara, R.; Fujita, K.; Yamaguchi, R. *J. Am. Chem. Soc.* **2012**, *134*, 3643.
(42) Wang, W.; Hull, J. F.; Muckerman, J. T.; Fujita, E.; Himeda, Y. *Energy Environ. Sci.* **2012**, *5*, 7923.
(43) DePasquale, J.; Nieto, I.; Reuther, L. E.; Herbst-Gervasoni, C.; Paul, J. J.; Mochalin, V.; Zeller, M.; Thomas, C. M.; Addison, A. W.; Papish, E. T. *Inorg. Chem.* **2013**, *52*, 9175.
(44) Ward, M. D.; McCleverty, J. A. *J. Chem. Soc., Dalton Trans.* **2002**, 275.
(45) Ringenberg, M. R.; Kokatam, S. L.; Heiden, Z. M.; Rauchfuss, T. B. *J. Am. Chem. Soc.* **2008**, *130*, 788.
(46) Nippe, M.; Khnayzer, R. S.; Panetier, J. A.; Zee, D. Z.; Olaiya, B. S.; Head-Gordon, M.; Chang, C. J.; Castellano, F. N.; Long, J. R. *Chem. Sci.* **2013**, *4*, 3934.
(47) Wilson, A. D.; Newell, R. H.; McNevin, M. J.; Muckerman, J. T.; Rakowski DuBois, M.; DuBois, D. L. *J. Am. Chem. Soc.* **2006**, *128*, 358.
(48) Dogutan, D. K.; McGuire, R.; Nocera, D. G. *J. Am. Chem. Soc.* **2011**, *133*, 9178.
(49) Costentin, C.; Drouet, S.; Robert, M.; Savéant, J. *J. Am. Chem. Soc.* **2012**, *134*, 11235.
(50) Bard, A. J.; Faulkner, L. R. *Electrochemical Methods: Fundamentals and Applications*; John Wiley & Sons, Inc.: New York, 2001.
(51) Concepcion, J.; Jurss, J.; Hoertz, P.; Meyer, T. *Angew. Chem., Int. Ed.* **2009**, *48*, 9473.
(52) Ryl, L. B.; Ronay, G. S.; Fowkes, F. M. *J. Phys. Chem.* **1958**, *62*, 798.
(53) Gustafson, R. L.; Martell, A. E. *J. Am. Chem. Soc.* **1959**, *81*, 525.
(54) Fabian, I. *Inorg. Chem.* **1989**, *28*, 3805.
(55) Garribba, E.; Micera, G.; Sanna, D.; Strinna-Erre, L. *Inorg. Chim. Acta* **2000**, *299*, 253.

(56) Mirceski, V.; Komorsky-Lovric, S.; Lovric, M. *Square-Wave Voltammetry: Theory and Application*; Springer-Verlag: Berlin, 2007.
(57) Osteryoung, J.; O'Dea, J. J. In *Electroanalytical Chemistry: A Series of Advances*; Bard, A. J., Ed.; Marcel Dekker, Inc.: New York, 1986; Vol. *14*, pp 209−308.
(58) Winkler, J. R.; Gray, H. B. *Struct. Bonding (Berlin)* **2012**, *142*, 17.
(59) Kolthoff, I. M.; Tomsicek, W. J. *J. Phys. Chem.* **1934**, *39*, 945.
(60) Frisch, M. J., et al. *Gaussian 09, Revision C. 01*; Gaussian, Inc.: Wallingford CT, 2010.
(61) Marenich, A. V.; Majumdar, A.; Lenz, M.; Cramer, C. J.; Truhlar, D. G. *Angew. Chem., Int. Ed.* **2012**, *51*, 12810.